

# Examining the interoperability of PPP-AR products

G. Seepersad and S. Bisnath  
*York University, Toronto, Canada*

## BIOGRAPHIES

Garrett Seepersad is a Ph.D. candidate at York University, Toronto, Canada, in the Department of Earth and Space Science and Engineering. He has completed his B.Sc. in Geomatics at the University of West Indies and his M.Sc. in Geomatics Engineering at York University. His area of research currently focuses on the development and testing of PPP functional, stochastic and error mitigation models.

Dr. Sunil Bisnath is an Associate Professor in the Department of Earth and Space Science and Engineering at York University in Toronto, Canada. His research interests include geodesy and precise GNSS positioning and navigation.

## ABSTRACT

Integer ambiguity resolution of carrier-phase measurements from a single receiver can be implemented by applying additional satellite products to mitigate the unmodeled satellite hardware delay. Interoperability of different PPP-AR products would allow the PPP user to transform independently generated PPP-AR products to obtain multiple fixed solutions of comparable precision and accuracy with limited changes required to the core PPP software. The ability to provide multiple solutions would increase the reliability of the solution for, e.g., real-time processing; if there were an outage in the generation of one set of PPP-AR products, the user could instantly switch streams to a different provider.

There are currently three main public providers of real-time products that enable PPP-AR. These included Scripps Institution of Oceanography, Natural Resources Canada and Centre national d'études spatiales. The research presented examines the PPP-AR products generated from the FCB (Fractional Cycle Bias) and IRC (Integer Receiver Clock) model that have been transformed into the DC (Decoupled Clock) format and applied within the PPP user solution. The novelty of the research is the solution analysis using the transformed product. The convergence time (time to

first fix and time to a pre-defined performance level), position precision (repeatability), position accuracy and solution outliers are examined. The temporal and spatial behaviour of these estimated terms are examined for the different products applied to understand the unmodeled effects that introduce incorrect solution fixes.

Unlike the fixed solution using the DC products, instantaneous convergence was not attained in the horizontal and vertical component when the transformed IRC and FCB products were utilized. In the horizontal component, the transformed IRC product took 10 minutes to attain the pre-defined threshold while the FCB product took 31 minutes in the horizontal component. A steady state was never attained, as jumps in the solution occurred at frequent intervals. The transformed IRC product had solution jumps every 15 minutes and the transformed FCB products had jumps in the solution every 30 to 45 minutes. The unstable solution from both transformed products are attributed to the magnitude of transformed products, as they were sub-nanoseconds in magnitude, whereas the DC products were few nanoseconds in magnitude.

## INTRODUCTION

Precise Point Positioning (PPP) requires a relatively long initialization period of at least a few tens of minutes for the carrier-phase ambiguities to converge to constant values and for the solution to reach its optimal precision. The carrier-phase signals are approximately two orders of magnitude more precise than the primary pseudorange signals. However, measurements of the carrier-phases are ambiguous, relative to those of the pseudoranges by an unknown number of integer cycles. In RTK, the integer nature of the carrier-phase ambiguities is uncovered by explicitly differencing simultaneous observations from multiple stations visible to the same satellites. Differencing of simultaneous observations can be thought of as an optimal correction method (Collins and Bisnath 2011), as the error sources are not modelled. Ambiguity resolution in PPP (PPP-AR) requires the hardware delays within the GPS measurements to be mitigated, which would allow for resolution of the

integer nature of the carrier-phase measurements (Laurichesse and Mercier 2007; Collins 2008; Mervart et al. 2008; Ge et al. 2008; Teunissen et al. 2010; Bertiger et al. 2010; Geng et al. 2012; Lannes and Prieur 2013). Resolution of these ambiguities convert the carrier-phases into precise pseudorange measurements, with measurement noise at the centimetre-to-millimetre level compared to the metre-to-decimetre-level of the direct pseudoranges (Collins et al. 2010). If the ambiguities could be isolated and estimated as integers, then there would be more information that could be exploited to accelerate convergence to give cm-level horizontal accuracy within an hour of data collection. Collins et al. (2008) and Laurichesse et al. (2009) saw improvements in hourly position estimates by 2 cm and Geng et al. (2010) saw noticeable hourly improvements from 1.5, 3.8 and 2.8 cm to 0.5, 0.5, 1.4 cm for north, east and up, respectively.

Integer ambiguity resolution of measurements from a single receiver can be implemented by applying additional satellite products, where the fractional component, representing the satellite hardware delay, has been separated from the integer ambiguities in a network solution. One method of deriving such products is to estimate the satellite hardware delay by averaging the fractional parts of the steady-state float ambiguity estimates (Ge et al. 2008), and the other is to estimate the pseudorange and carrier-phase clocks independently by fixing the undifferenced ambiguities to integers in advance (Collins 2008; Laurichesse et al. 2009). The initial application of ambiguity resolution to PPP was made by Ge et al. (2008) using the Uncalibrated Phase Delay (UPD) model, now called Fractional Cycle Bias (FCB) model (Geng et al. 2010; Geng et al. 2012). The FCB method estimates combined pseudorange/carrier-phase satellite hardware delays to remove the pseudorange satellite hardware delays from common clock estimates, such as those provided by the IGS. An alternative approach to PPP-AR was developed by Collins et al. (2008) called the Decoupled Clock (DC) model. The underlying concept of the DC model is the carrier-phase and pseudorange measurements are not synchronized with each other at the level of precision of the carrier-phase. The timing of the different observable must be considered separately, if they are to be processed together rigorously. The DC model is a reformulation of the ionosphere-free pseudorange and carrier-phase observation equations for GPS, when combined with the wide lane phase and narrow lane pseudorange observable, permits undifferenced ambiguity resolution of ambiguities (Collins 2008). The Integer Recovery Clocks (IRC) model presented by Mercier and Laurichesse (2007)

and Laurichesse and Mercier (2007) consists of daily averages of the wide lane biases and carrier-phase clocks. Zhang et al. (2011) presented a different approach to PPP-AR where the user is provided with the satellite hardware delay for the L1 and L2 carrier-phase signals. In Teunissen and Khodabandeh (2015), the model presented by Zhang et al. (2011) is referred to as the Common Clock (CC-1).

Similar positioning performances have been demonstrated amongst the three methods, DC (Collins et al. 2010), FCB (Ge et al. 2008; Geng et al. 2009) and IRC (Laurichesse et al. 2009). Studies such as Geng et al. (2010), Shi and Gao (2013), and Teunissen and Khodabandeh (2015) have identified the differences and the fundamental similarities between the methods. For the PPP user, the mathematical model is similar; the different PPP-AR products contain the same information and as a result would allow for one-to-one transformations, allowing interoperability of the PPP-AR products (Teunissen and Khodabandeh 2015). The advantage of interoperability of the different PPP-AR products would be to allow the PPP user to transform independently generated PPP-AR products to obtain multiple fixed solutions of comparable precision and accuracy. The ability to provide multiple solutions would increase the reliability of the solution for, e.g., real-time processing; if there were an outage in the generation of the PPP-AR products, the user can instantly switch streams to a different provider. The research presented examines the PPP-AR products generated from the FCB and IRC model that have been transformed into the DC format and applied within the PPP user solution. The novelty of the research is the solution analysis using the transformed product. The convergence time (time to first fix and time to a pre-defined performance level), position precision (repeatability), position accuracy and solution outliers would be examined. The temporal and spatial behaviour of these estimated terms is examined for the different products applied to understand the unmodeled effects that introduced incorrect solution fixes.

## OVERVIEW PPP-AR TECHNIQUES AND PRODUCTS

The standard GPS dual-frequency pseudorange and carrier-phase observation equations are presented in equations (1) and (2). Where  $i$  denotes the frequency dependent GPS measurements frequencies  $L1$  or  $L2$ .  $ps$  represents the single difference satellites where  $p$  represents the reference satellite,  $s$  represents the other tracked satellite and  $u$  represents the user position.

$$\Delta\phi_{u,i}^{ps} = \Delta\rho_u^{ps} - \mu_i t_{u,i}^{ps} - dt^{ps} + \lambda_i z_{u,i}^{ps} - \lambda_i \delta_i^{ps} \quad (1)$$

$$\Delta p_{u,i}^{ps} = \Delta\rho_u^{ps} + \mu_i t_{u,i}^{ps} - dt^{ps} - d_i^{ps} \quad (2)$$

$\Delta\phi_{u,i}^{ps}$  and  $\Delta p_{u,i}^{ps}$  represents the single differenced carrier-phase and pseudorange measurements.  $\Delta\rho_u^{ps}$  is the geometric range between single difference satellites and user position and tropospheric delay.  $t_u^{ps}$  is the first order slant ionospheric delay and  $\mu_i$  is the frequency dependent coefficient.  $dt^{ps}$  is the single differenced satellite clock and  $d_i^{ps}$  is the single differenced pseudorange hardware delay.  $z_{u,i}^{ps}$  is the single differenced ambiguity and  $\delta_i^{ps}$  is the single differenced carrier-phase hardware delay which are expressed in cycles and scaled by the wavelength  $\lambda_i$ .

The user observation equations (1) and (2) do not contain sufficient information to solve for an integer ambiguity resolved user position. Ambiguity resolution would become possible if information about the satellite clocks and hardware delays were provided to the user. Using such externally provided information ( $dt^{ps}$ ,  $\delta^{ps}$ ,  $d^{ps}$ ) to correct the observations as

$$\Delta\phi_{u,i}'^{ps} = \Delta\phi_{u,i}^{ps} + dt^{ps} + \lambda_i \delta_i^{ps} \quad (3)$$

$$\Delta p_{u,i}'^{ps} = \Delta p_{u,i}^{ps} + dt^{ps} + d_i^{ps} \quad (4)$$

results in user-equations that take the form

$$\Delta\phi_{u,i}'^{ps} = \Delta\rho_{u,i}^{ps} - \mu_i t_{u,i}^{ps} + z_{u,i}^{ps} \quad (5)$$

$$\Delta p_{u,i}'^{ps} = \Delta\rho_{u,i}^{ps} + \mu_i t_{u,i}^{ps} \quad (6)$$

By utilizing externally provided corrections the user's system of observation equations (5) and (6) can be solved (Teunissen and Khodabandeh 2015).

Presented in the following section is an overview of the different public providers of products that enable PPP-AR, the products and how they are applied to the PPP user equations.

### Public PPP-AR products

Currently, there are three main public providers of products that enable PPP-AR. These include Scripps Institution of Oceanography (Geng and Bock 2013; Scripps 2015) which

provides regional real-time FCB products, Natural Resources Canada (Collins 2008; NRCAN 2015) which provides post-processed and real-time DC products and Centre national d'études spatiales (Laurichesse et al. 2009; CNES 2015) which also provides post-processed and real-time IRC products.

### Fractional Cycle Bias (FCB) model

The initial application of ambiguity resolution to PPP was made by Ge et al. (2008) using the Fractional Cycle Bias (FCB) model. The FCB method estimates the hardware delay by averaging the fractional parts of the steady-state float ambiguity estimates (Ge et al. 2008) to be removed from common satellite clock estimates. Presented in equations (7) to (9) is the application of the FCB products  $\tilde{dt}^{ps}$ ,  $\tilde{a}_{q,1}^{ps}$  and  $\tilde{a}_{q,W}^{ps}$  where  $\sim$  represents these products were estimated from within the network solution and  $\approx$  represents the corrected user equations. *IF* represents the ionospheric free linear combination and *WN* represents the Melbourne-Wübbena combination.

$$\Delta\tilde{\phi}_{u,IF}^{ps} = \Delta\phi_{u,IF}^{ps} + \tilde{dt}^{ps} - \lambda_N \tilde{a}_{q,1}^{ps} - \frac{\lambda_2}{\mu_{12}} \tilde{a}_{q,W}^{ps} \quad (7)$$

$$\Delta\tilde{p}_{u,IF}^{ps} = \Delta p_{u,IF}^{ps} + \tilde{dt}^{ps} \quad (8)$$

$$\Delta\tilde{\phi}_{u,WN}^{ps} = \Delta\phi_{u,WN}^{ps} - \lambda_W \tilde{a}_{q,W}^{ps} \quad (9)$$

Presented in Figure 1 is the relative satellite clock error,  $\tilde{dt}^{ps}$  for PRN 10 with respect to satellite PRN 27 from 0 to 4 hours 10 minutes and PRN 6 from 8 hours 45 minutes to 24 hours. The real-time products provided by Scripps are regional, thus data are provided to the user only when satellite coverage is available over the greater California region. The satellite clock error are transmitted at a 1 Hz data rate.

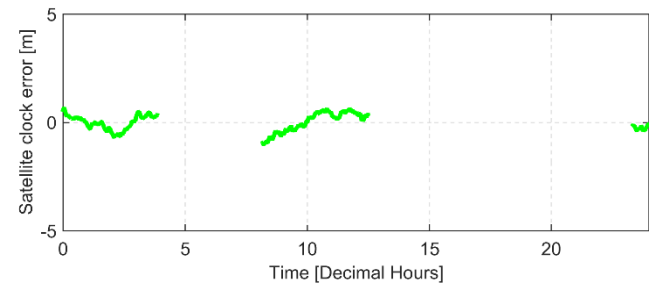


**Figure 1: Relative satellite clock correction provided by Scripps on DOY 28 of 2015 for PRN 10 (relative to PRN 6 and 27). Linear trend has been removed. All units are in metres.**

Presented in Figure 2 is the narrow lane  $\tilde{a}_{q,1}^{ps}$  and the wide lane FCB correction,  $\tilde{a}_{q,W}^{ps}$  for PRN 10. Similarly to the clock product, the narrow lane FCB has data gaps due to the regional nature of the products. The products are transmitted at a 5 second data rate. The wide lane FCBs  $\tilde{a}_{q,W}^{ps}$  are transmitted once every 48 hours. Geng (2010) describes the wide lane FCBs are very stable over several days, or even a few months.

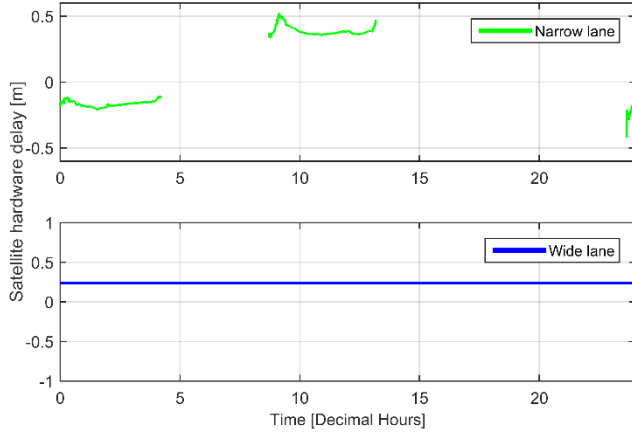


**Figure 2: “Narrow lane” (upper subplot) and wide lane (lower subplot) FCB provided by Scripps on DOY 28 of 2015 for PRN 10. All units are in metres.**

### Decoupled Clock (DC) model

The underlying concept of the decoupled clock model presented by Collins et al. (2008) is the carrier-phase and pseudorange measurements are not synchronized with each other at equivalent level of precision. The timing of the different observables must be considered separately, if they are to be processed together rigorously. The decoupled clock model is a reformulation of the ionosphere-free carrier-phase and pseudorange observation equations presented in equations (10) and (11). When combined with the narrow lane pseudorange, equation (12) and the wide lane phase, equation (13) allows for ambiguity resolution. The DC products transmitted to the user are  $\delta\tilde{t}_{IF}^{ps}$ ,  $d\tilde{t}^{ps}$  and  $\tilde{\delta}_{WN}^{ps}$ .

$$\Delta\tilde{\phi}_{u,IF}^{ps} = \Delta\phi_{u,IF}^{ps} + \delta\tilde{t}_{IF}^{ps} \quad (10)$$

$$\Delta\tilde{p}_{u,IF}^{ps} = \Delta p_{u,IF}^{ps} + d\tilde{t}^{ps} \quad (11)$$

$$\Delta\tilde{p}_{u,NL}^{ps} = \Delta p_{u,NL}^{ps} + \delta\tilde{t}_{IF}^{ps} + \lambda_{WL}\tilde{\delta}_{WN}^{ps} \quad (12)$$

$$\Delta\tilde{\phi}_{u,WL}^{ps} = \Delta\phi_{u,WL}^{ps} + \delta\tilde{t}_{IF}^{ps} \quad (13)$$

Where  $NL$  represents the narrow lane linear combination and  $WL$  represents the wide lane linear combination. The reformulated DC model using  $\Delta\tilde{p}_{u,NL}^{ps}$  and  $\Delta\tilde{\phi}_{u,WL}^{ps}$  rather than  $\Delta\tilde{\phi}_{u,WN}^{ps}$  was carried out to allow the PPP user to utilize the estimation of the slant ionospheric term for instantaneous re-convergence. (Collins and Bisnath 2011)

Presented in Figure 3 is the relative satellite phase clock error,  $\delta\tilde{t}_{IF}^{ps}$  for PRN 10 with respect to satellite PRN 27.

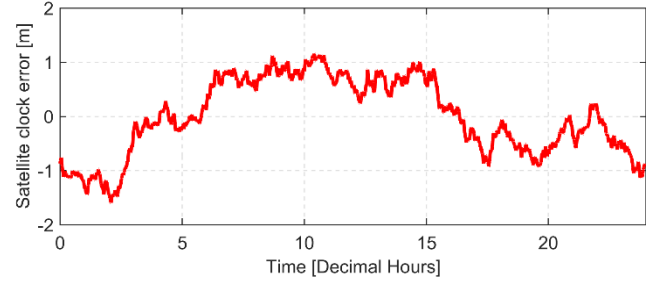


**Figure 3: Relative satellite phase clock correction provided by NRCan on DOY 28 of 2015 for PRN 10 (relative to PRN 27). Linear trend has been removed. All units are in metres.**

Figure 4 illustrates the relative satellite pseudorange clock error,  $(d\tilde{t}^{ps} - \delta\tilde{t}_{IF}^{ps})$  and the relative wide lane clock error,  $(\tilde{\delta}_{WN}^{ps} - \delta\tilde{t}_{IF}^{ps})$  for PRN 10. The relative satellite pseudorange and wide lane clock has a larger standard deviation of 0.463 m and 0.119 m, respectively. In contrast to the FCB and IRC products, has a larger standard deviation because in the estimation of the products they are unconstrained and unfiltered. All products are transmitted at a 30 second data rate.

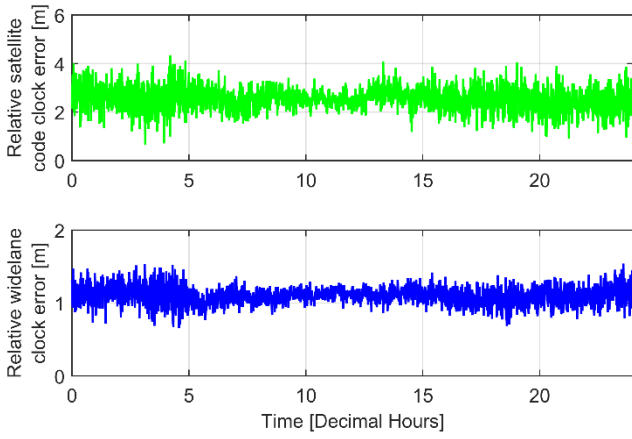


**Figure 4: Relative code clock error (upper figure) and wide lane (lower figure) DC provided by NRCan on DOY 28 of 2015 for PRN 10. All units are in metres.**

### Integer Recovery Clock (IRC) model

The integer recovery clocks presented by Mercier and Laurichesse (2007) and Laurichesse and Mercier (2007) estimate constant daily wide lane pseudorange/carrier-phase hardware delays by averaging arc-dependent estimates. Using float-solution estimates of the range parameters, narrow lane ambiguity resolution is performed and the ionosphere-free satellite carrier-phase clocks are estimated. Laurichesse (2014) adopted a state space uncombined representation of their products, as such, satellite hardware delay is provided for each observable ( $\tilde{\delta}_i^{ps}$ ,  $\tilde{d}_i^{ps}$ ) and satellite pseudorange clock ( $\tilde{dt}^{ps}$ ).

$$\Delta\tilde{\phi}_{u,i}^{ps} = \Delta\phi_{u,i}^{ps} + \tilde{dt}^{ps} + \lambda_i \tilde{\delta}_i^{ps} \quad (14)$$

$$\Delta\tilde{p}_{u,i}^{ps} = \Delta p_{u,IF}^{ps} + \tilde{dt}^{ps} + \tilde{d}_i^{ps} \quad (15)$$

Presented in Figure 5 is the relative satellite pseudorange clock error,  $\tilde{dt}^{ps}$  for PRN 10 with respect to satellite PRN 27.

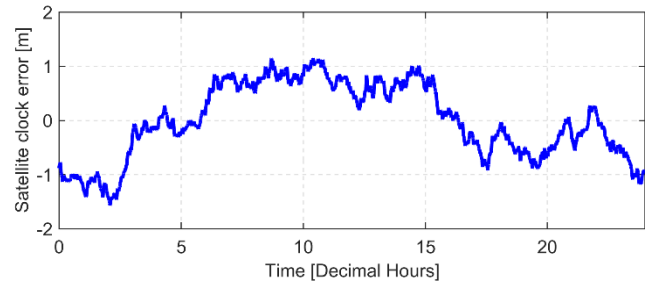


**Figure 5: Relative satellite clock correction provided by CNES on DOY 28 of 2015 for PRN 10 (relative to PRN 27). Linear trend has been removed. All units are in metres.**

Presented in Figure 6 are the observable dependent satellite hardware delays for the pseudorange ( $\tilde{d}_i^{ps}$ ) and carrier-phase measurements ( $\tilde{\delta}_i^{ps}$ ).  $\tilde{d}_i^{ps}$  are assumed constant over a 24 hour period and the  $\tilde{\delta}_i^{ps}$  are transmitted at a 5 second data rate. All products are transmitted at a 30 second data rate.

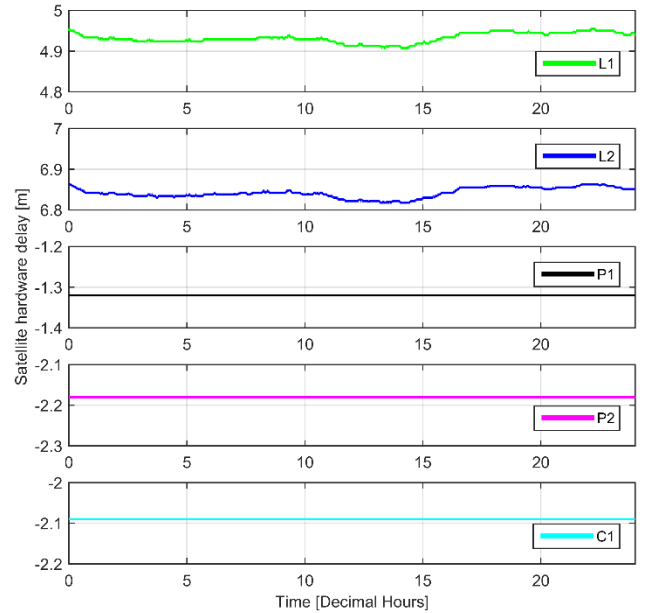


**Figure 6: Observable dependent satellite hardware delay for PRN 10 IRC provided by CNES on DOY 28 of 2015 for PRN 10.**

## Summary

The user implementation examines the three public providers of products to enable real-time PPP-AR are listed in Table 1. The criteria includes the different products transmitted, data rate transmitted, latency and different assumptions made.

**Table 1: Comparison of different public providers of real-time products to enable PPP-AR.**

	Fractional Cycle Bias (FCB) model	Decoupled Clock (DC) model	Integer Recovery Clock (IRC) model
<b>PPP-AR Products</b>	$d\tilde{t}_{IF}^{ps}$ - code clock $\tilde{a}_{q,W}^{ps}$ - wide lane $\tilde{a}_{q,1}^{ps}$ - narrow lane	$\delta\tilde{t}_{IF}^{ps}$ - phase clock $d\tilde{t}_{IF}^{ps}$ - code clock $\tilde{\delta}_{WN}^{ps}$ - wide lane clock	$d\tilde{t}_{IF}^{ps}$ - code clock $\tilde{\delta}_{i}^{ps}$ -phase hardware delay $\tilde{d}_{i}^{ps}$ - code hardware delay
<b>Data rate</b>	$d\tilde{t}^{ps}$ - 5 secs $\tilde{a}_{q,1}^{ps}$ - 1 sec $\tilde{a}_{q,W}^{ps}$ - 2 days	$\delta\tilde{t}_{IF}^{ps}$ - 30 secs $d\tilde{t}^{ps}$ - 30 secs $\tilde{\delta}_{WN}^{ps}$ - 30 secs	$d\tilde{t}^{ps}$ - 30 sec $\tilde{\delta}_{i}^{ps}$ - 5 secs $\tilde{d}_{i}^{ps}$ - daily
<b>Assumptions</b>	Constant $\tilde{a}_{q,W}^{ps}$ are estimated every 48 hours by averaging arc-dependent estimates. No constraints applied to estimating $\tilde{a}_{q,1}^{ps}$ .	No constraints or smoothing applied.	Constant $\tilde{\delta}_{WN}^{ps}$ are estimated every 24 hours by averaging arc-dependent estimates.
<b>PPP user model</b>	P3,L3,P6,L4	P3,L3,P6,L4	P3,L3,P6,L4
<b>P1/P2 correction</b>			$\tilde{d}_{i}^{ps}$
<b>L1/L2 correction</b>			$\tilde{\delta}_{i}^{ps}$
<b>NL correction</b>	$\tilde{a}_{q,1}^{ps}$		
<b>WL correction</b>	$\tilde{a}_{q,W}^{ps}$	$\tilde{\delta}_{WN}^{ps}$	

## PRODUCT TRANSFORMATION

While the different strategies (FCB, FC, IRC) make different assumptions, there are fundamental similarities between the different strategies. For the PPP user, the mathematical model is similar; the different PPP-AR products contain the same information and as a result would allow for a one-to-one transformation, allowing interoperability of the PPP-AR products (Teunissen and Khodabandeh 2015). The advantage of interoperability of the different PPP-AR products would be to allow the PPP user to transform independently generated PPP-AR products to obtain multiple fixed solutions of comparable precision and accuracy. The ability to provide multiple solutions would increase the reliability of the solution for, e.g., real-time processing; if there was an outage in the generation of the PPP-

AR products, the user can instantly switch streams to a different provider. The following sections examines the transformation matrix used to transform the IRC and FCB products to the DC format.

### Fractional Cycle Bias

The FCB products consist of  $d\tilde{t}^{ps}$ ,  $\tilde{a}_{q,1}^{ps}$  and  $\tilde{a}_{q,W}^{ps}$  which has been estimated in the network solution utilizing IGS ultra rapid orbit and clock products. The fundamental differences between the FCB and DC is that  $\tilde{a}_{q,1}^{ps}$  is not determined in the DC method, but assimilated within the clock estimates. Also,  $\tilde{a}_{q,W}^{ps}$  are assumed constant over a 48 hour time period whereas in the DC method the  $\tilde{\delta}_{WN}^{ps}$  is neither constrained nor smoothed. Presented in equation (16) is the

transformation matrix used to transform from FCB to DC model which was presented in Teunissen and Khodabandeh (2015).

$$\begin{bmatrix} \tilde{d}_{IF}^{ps} \\ \delta \tilde{t}_{IF}^{ps} \\ \tilde{\delta}_{WN}^{ps} \end{bmatrix} = \begin{bmatrix} 1 & 0 & 0 \\ -\frac{1}{\lambda_N} & \frac{1}{\lambda_N} & -\frac{\lambda_1}{\lambda_2 - \lambda_1} \\ -\frac{1}{\lambda_N} & \frac{1}{\lambda_N} & -\frac{\lambda_2}{\lambda_2 - \lambda_1} \end{bmatrix}^{-1} \begin{bmatrix} 1 & 0 & 0 \\ 0 & -1 & \frac{\lambda_1}{\lambda_2 - \lambda_1} \\ 0 & -1 & \frac{\lambda_2}{\lambda_2 - \lambda_1} \end{bmatrix} \begin{bmatrix} \tilde{d}_{IF}^{ps} \\ \tilde{a}_{q,1}^{ps} \\ \tilde{a}_{q,W}^{ps} \end{bmatrix} + \begin{bmatrix} 0 \\ z_1 \\ z_w \end{bmatrix} \quad (16)$$

### Integer Recovery Clock

The original IRC method (Laurichesse and Mercier 2007; Mercier and Laurichesse 2007) was a decouple like approach where independent clocks were used for the pseudorange and carrier-phase measurements and daily wide lane satellite hardware delays were estimated. A redefined model was presented Laurichesse (2014) where a state spaced approach was presented such that one phase bias per phase observable is identified and broadcasted. The primary benefit of such an approach is interoperability allowing the network and user side implement different ambiguity resolution methods. Presented in Laurichesse (2014) is the transformation of the original IRC ( $\delta \tilde{t}_{IF}^{ps}$  and  $\tilde{\delta}_{WN}^{ps}$ ) to  $\tilde{\delta}_{1,1}^{ps}$  and  $\tilde{\delta}_{2,2}^{ps}$ . The inverse transformation in equation (17) was has been utilized to transform the transmitted  $\tilde{\delta}_{1,1}^{ps}$  and  $\tilde{\delta}_{2,2}^{ps}$  products into its original  $\delta \tilde{t}_{IF}^{ps}$  and  $\tilde{\delta}_{WN}^{ps}$  components.

$$\begin{bmatrix} \delta \tilde{t}_{IF}^{ps} \\ \tilde{\delta}_{WN}^{ps} \end{bmatrix} = \begin{bmatrix} 1 & 0 \\ 0 & \gamma_2 - 1 \end{bmatrix}^{-1} \left( \begin{bmatrix} -\lambda_2 & 1 \\ \gamma_2 \lambda_1 - \lambda_2 & \gamma_2 \lambda_1 - \lambda_2 \\ \gamma_2 \lambda_1 & 1 \\ \gamma_2 \lambda_1 - \lambda_2 & \gamma_2 \lambda_1 - \lambda_2 \end{bmatrix}^{-1} \begin{bmatrix} \tilde{\delta}_{1,1}^{ps} \\ \tilde{\delta}_{2,2}^{ps} \end{bmatrix} - \begin{bmatrix} -d_{12} \\ 0 \end{bmatrix} \right) \quad (17)$$

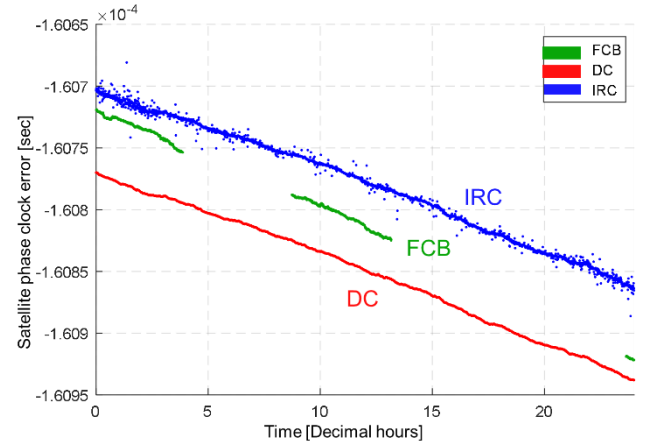
Where  $d_{12}$  represents  $\frac{(\lambda_1 - \lambda_2)(\lambda_1 d_1 - \lambda_2 d_2)}{\lambda_1 + \lambda_2}$

### Analysis of transformed products

Presented in Figures 7 to 9 are the transformed products to the DC format. The presented format was selected because it represents the nature of which the real-time DC products are transmitted. The philosophy of the DC model refers to the satellite hardware delay as an unmodeled timing error and as such, the satellite carrier-phase clocks in Figure 7 are in units of seconds and Figures 8 and 9 are in units of nanoseconds. Nanoseconds was selected because of the

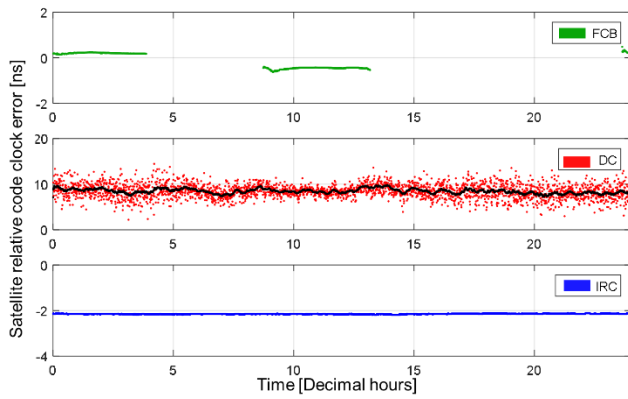
magnitude of the relative satellite pseudorange and wide lane clock error, as well as being more bandwidth efficient.

Figure 7 illustrates the transformed FCB and IRC to the DC satellite carrier-phase clock. Unlike the earlier illustrations of the relative satellite clock errors, these are “absolute” satellite clock errors as they are not differenced with respect to a reference satellite. The data gaps in the FCB products are as expected because of the regional nature of the products. Unlike the DC and IRC products, the FCB pseudorange clocks illustrate different trends for example between hours 3 and 4. IRC and DC satellite phase clocks closely agree with a difference of relative products being 2.11 ns. The noise illustrated in the IRC clock can be removed by either filtering or differencing with respect to another satellite clock.



**Figure 7: Transformed FCB (upper) and IRC (lower) satellite phase clock correction on DOY 28 of 2015 for PRN 10. DC (middle) was included for comparison. All units are in seconds.**

Presented in Figure 8 is the relative satellite clock error ( $\tilde{d}_{IF}^{ps} - \delta \tilde{t}_{IF}^{ps}$ ) for the transformed FCB (upper subplot) and IRC (lower subplot) products. For the original DC product (middle subplot) a simple moving average filter was applied with a bin size of 5 minutes, to reduce the noise and illustrate the underlying equipment delay. The relative satellite clock error represents the difference between the pseudorange and carrier-phase clocks. The distinct differences of the products are easily visible, such as the filtering present within FCB and IRC products in contrast to the DC. The underlying relative satellite clock error is also significantly different in contrast to the DC product, such that FCB and IRC has an average relative satellite clock error of  $-0.041 \pm 0.101$  ns and  $-0.645 \pm 0.0045$  ns, respectively, whereas the DC has an average of  $8.465 \pm 1.546$  ns.



**Figure 8: Transformed FCB (upper) and IRC (lower) to code-phase relative clock correction on DOY 28 of 2015 for PRN 10. DC (middle) was included for comparison. Linear trend has been removed. All units are in seconds.**

Presented in Figure 9 is the relative satellite wide lane clock error for the transformed FCB (upper figure) and IRC (lower figure) products. For the original DC product (middle subplot) a simple moving average filter was applied with a bin size of 5 minutes, to reduce the noise and illustrate the underlying equipment delay. The relative satellite clock error represents the difference between the wide lane clocks and phase clocks. Similar to the relative satellite clock error, the differences in the transformed relative satellite wide lane clock error are noticeably different. As expected, the transformed FCB has a constant wide lane estimate of  $-0.24$  ns, whereas the transformed IRC and DC had an average wide lane of  $0.0589 \pm 0.002$  and  $3.6704 \pm 0.34$  ns, respectively.

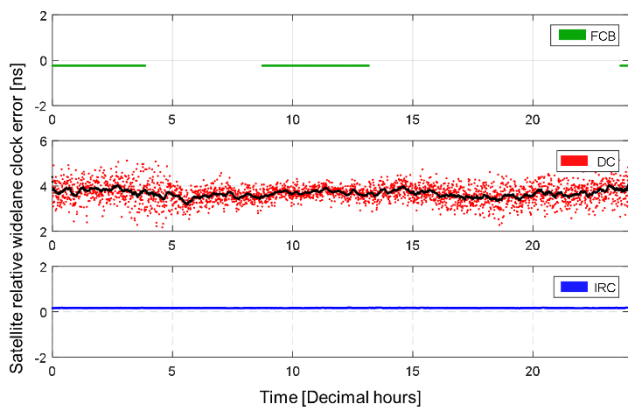


**Figure 9: Transformed FCB (upper) and IRC (lower) to code-phase relative wide lane clock correction on DOY 28 of 2015 for PRN 10. DC (middle) was included for comparison. Linear trend has been removed. All units are in seconds.**

## DATASET AND PROCESSING PARAMETERS

GPS data from 5 stations IGS stations observed during-DOY 25 to 31, GPS week 1829, of 2015 were processed using the York-PPP software (Seepersad 2012; Aggrey 2015). York-PPP was developed based on the processing engine used by the on-line CSRS-PPP service (NRCAN 2013). The GPS stations selected were within the California region. These sites were selected to allow utilization of the regional FCB products. The distribution of the sites are illustrated in Figure 10. Dual-frequency receivers tracking either the C/A or P(Y) - code on L1 were used. For receivers that do not record the P1 observable, the P1C1 code bias correction was applied. Settings used for the evaluation include the ionosphere-free combination of L1 and L2 data, 2 m and 15 mm a priori standard deviations for pseudorange and carrier-phase observations, respectively, and a  $10^\circ$  elevation cut-off angle.

The reference stations were analyzed in static mode. Receiver clocks were estimated epoch-by-epoch. The zenith tropospheric delays were also estimated each epoch with a random walk co-efficient of  $2 \text{ cm}/\sqrt{\text{hour}}$ . The station coordinates were initialized using a pseudorange only solution with an initial constraint of 10 m. The IGS absolute antenna model file was used and ocean loading coefficients were obtained from Scherneck (2013) for each of the sites processed.

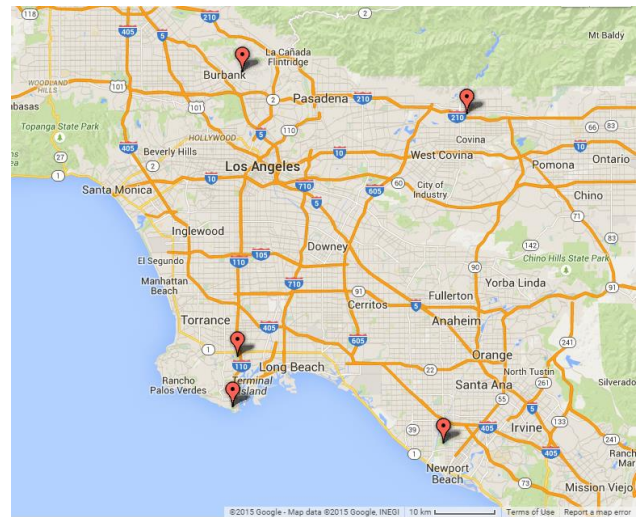


**Figure 10: Distribution of the selected 5 IGS stations observed during DOY 25 to 31, GPS week 1829, of 2015.**

Presented in Figure 11 is the varying convergence periods at the site BRAN on DOY 30 for the “float” and “fixed” solution. Where fixed represents the ambiguity resolved

solution and float the unresolved solution. A stringent convergence threshold of 5 cm was set to examine the time the solution took to converge. For the float solution, the peak time occurred within the first minute with an overshoot of 7.2 m. While the predefined threshold was attained after 30 minutes of processing, the settling time was over 2 hours to attain a steady state. The fixed solution, the peak of 2 minutes with an overshoot of only 5 cm while also attaining the predefined threshold. The settling time took 7 minutes to attain a steady state.

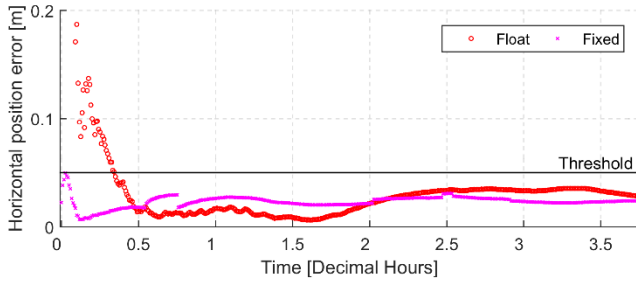


**Figure 11: Site BRAN DOY 30 of 2015 located in Burbank, California, illustrating the different between the “float” and “fixed” solution in the horizontal component.**

Figure 12 illustrates the vertical position error for the float and fixed PPP solution. Similar to horizontal component a 5 cm threshold is placed. For the float solution, the peak time occurred after 30 secs with an overshoot of 10.8 m. Similar to the horizontal component, the predefined threshold was attained after 30 minutes of processing and the settling time took 2.5 hours to attain a steady state. The fixed solution attained a peak time after 2 minutes with an overshoot of 36 cm. The predefined threshold was attained instantly and the settling time was after 8 minutes where a steady state was attained.

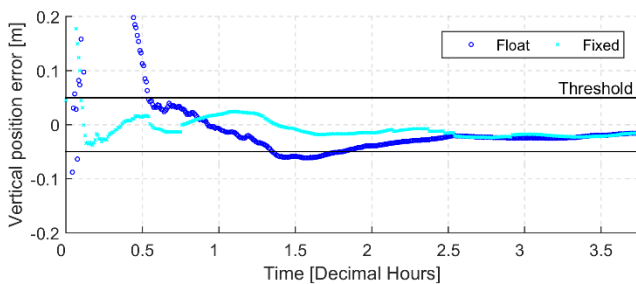


**Figure 12: Site BRAN DOY 30 of 2015 located in Burbank, California, illustrating the different between the “float” and “fixed” solution in the vertical component. All units are in metres.**

## PERFORMANCE OF TRANSFORMED PRODUCTS

One of the metrics used to examine the performance of the transformed products was to examine the quality of the solution in the position domain. The solutions were examined in regards of convergence time to the pre-defined threshold and position stability. The site BRAN on DOY 30 of 2015 was selected as it reflected the performance of the datasets processed.

Unlike the fixed solution provided using the DC products, instantaneous convergence was not attained in the horizontal (Figure 13) and vertical (Figure 14) component when the transformed IRC and FCB products were utilized. In the horizontal component, the transformed IRC product took 10 minutes to attain the predefined threshold while the FCB product took 31 minutes in the horizontal component. A steady state was never truly attained, as jumps in the solution occurred at frequent intervals. The transformed IRC product had solution jumps every 15 minutes and the transformed FCB products had jumps in the solution every 30 to 45 minutes.

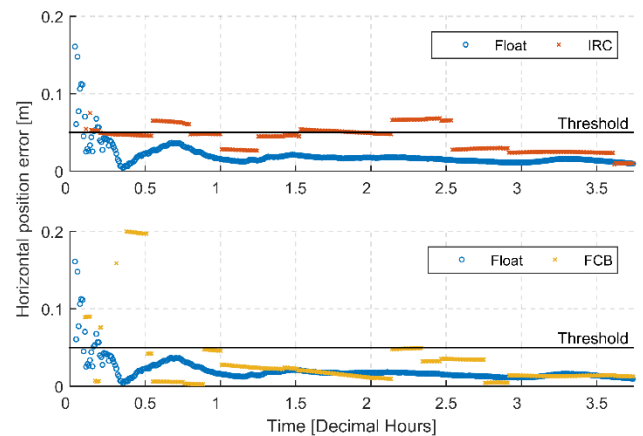


**Figure 13: Site BRAN DOY 30 of 2015 located in Burbank, California, illustrating the performance of the fixed solution in the horizontal component using the DC and transformed products. Transformed IRC and FCB products are used in upper and lower subplots respectively. All units are in metres.**

These trends were also noted in the vertical component. With the transformed IRC products, convergence was momentarily attained from decimal hours 0.1 to 0.55 but was only met again after 1 hour. For the transformed FCB products, solution was attained after 10 minutes of processing but was lost after 0.75 hours of processing and took an additional hour of processing for the pre-defined threshold to be attained.

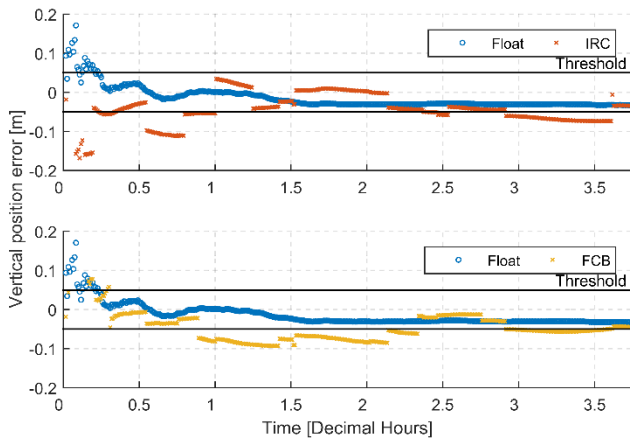


**Figure 14: Site BRAN DOY 30 of 2015 located in Burbank, California, illustrating the performance of the fixed solution in the vertical component using the DC and transformed FCB and IRC products. Transformed IRC and FCB products are used in upper and lower subplots respectively. All units are in metres.**

When the transformed products were applied, the solutions did have a smaller overshoot and shorter peak time, after convergence than the float solutions. In regards to performance and stability, the float attained a faster convergence and maintained a steady state for the entire data arc. Presented in Table 2 is the statistics from BRAN DOY 30 of 2015 based on initial 4 hour period. Larger biases and standard deviation of the float solution is attributed to the magnitude of the overshoot during initialization.

**Table 2: Summary statistics of float and fixed solution produced using the different PPP-AR products (DC, IRC and FCB) during convergence period. Statistics based on IGS station BRAN DOY 82 of 2015. All units are in millimetres.**

Units [mm]	Mean		Std	
	Horizon-tal	Verti-cal	Horizon-tal	Verti-cal
Float	57	41	339	481
DC	23	-5	5	40
IRC	50	-29	117	132
FCB	46	-39	139	105

### CHALLENGES OF INTEROPERABILITY OF PPP-AR PRODUCTS

Interoperability of the different PPP-AR products is a challenging task due to the public availability of different qual-

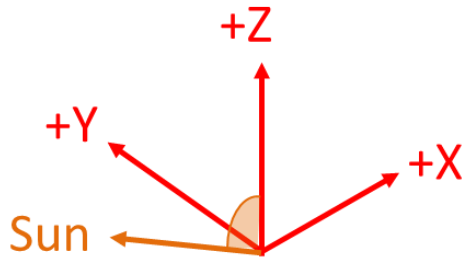
ity of products, limited literature documenting the conventions adopted within the network solution of the providers and unclear definitions of the corrections.

Presented in Table 3 is a summary of the different qualities of the products that was utilized within the study making it challenging perform a consistent comparison. IRC products were generated from a network of reference stations globally distributed and in real-time. Similar to the IRC, the DC products were generated from a global network of solutions but post-processed and the FCB was based on a regional network of reference stations but was available in real-time. Post-processed orbits and clocks have an accuracy of  $\sim 2.5$  cm and  $\sim 75$  ps respectively whereas the predicted half of ultra-rapid orbits and clocks have an accuracy of  $\sim 5$  cm and  $\sim 3$  ns respectively. While it is evident in existing literature PPP-AR is possible in real-time, the solution is more sensitive to changes experienced by the PPP user solution such as varying local conditions and satellite geometry. The sensitivity is illustrated in Figure 13 and Figure 14 as solution jumps typically occur when there is a change in the number of satellites.

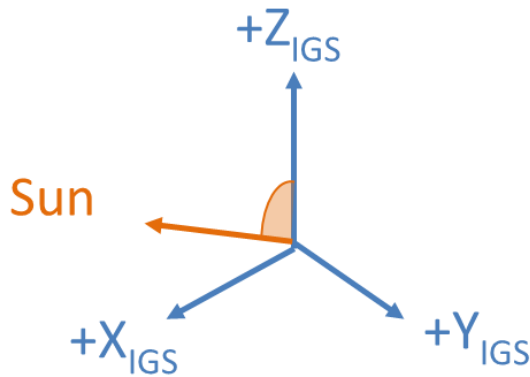
**Table 3: Summary of the different quality of products provided by public providers to enable PPP-AR**

	Regional	Global	Real Time	Post processed
IRC		X	X	
DC		X		X
FCB	X		X	

The general assumption when PPP-AR products are estimated within the network, assumes the PPP user would follow similar conventions when utilizing the products. Consequences of different conventions adopted may result in incorrect ambiguities being resolved. For example, if inconsistent satellite antenna convention is adopted between the network and user, when phase wind-up corrections are applied, fractional cycles would be introduced. Presented in Figure 15 is the orientation of the spacecraft body frame for GPS Block IIR/IIR-M satellites provided in the manufacturer specifications, subplot (a) and adopted within the IGS axis convention, subplot (b). The difference between the manufacturer specifications and IGS axis convention is the orientation of the X, Y – axis. For more details on the conventions for constellation-specific spacecraft body frames can be found in Montenbruck (2015).



(a) Manufacturer specifications



(b) IGS axis convention

**Figure 15: Orientation of the spacecraft body frame for GPS Block IIR/IIR-M satellites. Sub-plot (a) refers to the manufacturer specification system while sub-plot (b) refers to the IGS axis conventions (Montenbruck et al. 2015).**

## CONCLUSIONS

For the PPP user, the mathematical model to enable and ambiguity resolved solution is similar; the different PPP-AR products contain the same information and as a result would allow for a one-to-one transformation, allowing interoperability of the PPP-AR products. The advantage of interoperability of the different PPP-AR products would be to allow the PPP user to transform independently generated PPP-AR products to obtain multiple fixed solutions of comparable precision and accuracy. The ability to provide multiple solutions would increase the reliability of the solution for, e.g., real-time processing; if there was an outage in the generation of the PPP-AR products, the user can instantly switch streams to a different provider.

The three main public providers of products that enable PPP-AR were examined. These were included Scripps Institution of Oceanography which provided regional real-time FCB products, Natural Resources Canada which provided post-processed and real-time DC products and Centre national d'études spatiales which also provided post-processed and real-time IRC products. To examine the performance of the transformed products GPS data from 5 stations IGS stations observed during DOY 25 to 31, GPS week 1829, of 2015. The GPS stations selected were within the California region to allow to use of the regional FCB products. A stringent convergence threshold of 5 cm was set to examine the time the solution took to converge. The YorkU-PPP engine was originally designed for processing the DC products. In the horizontal component, on average took 7 minutes to attain convergence and a steady state. In the vertical convergence and a steady state took 8 minutes.

Unlike the fixed solution using the DC products, instantaneous convergence was not attained in the horizontal and vertical component when the transformed IRC and FCB products were utilized. In the horizontal component, the transformed IRC product took 10 minutes to attain the predefined threshold while the FCB product took 31 minutes in the horizontal component. A steady state was never attained, as jumps in the solution occurred at frequent intervals. The transformed IRC product had solution jumps every 15 minutes and the transformed FCB products had jumps in the solution every 30 to 45 minutes. The unstable solution from both transformed products are attributed to the magnitude of the relative satellite code and wide lane clock error. The underlying relative satellite clock error was significantly different in contrast to the DC product, such that FCB and IRC has an average relative satellite clock error of  $-0.041 \pm 0.101$  ns and  $-0.645 \pm 0.0045$  ns respectively whereas the DC has an average of  $8.465 \pm 1.546$  ns. For the transformed relative wide lane clock error, FCB has a constant wide lane estimate of  $-0.24$  ns, whereas the transformed IRC and DC had an average wide lane of  $0.0589 \pm 0.002$  and  $3.6704 \pm 0.34$  ns respectively. Additional refinement of the model required as the satellite hardware delay has not been completely mitigated. Mismodeling of the hardware delay was absorbed by the ambiguity terms causing incorrect fixed solutions to be present.

## FUTURE WORK

Future work would consist of refinement of the proposed transformation models to include the mismodeled effects

thus providing user a more reliable solution. The functional model needs to be further examined to ensure the corrections were applied consistently. Further analysis of the instability of the user solution is required, as solution jumps typically occur when there was a change in the number of satellites. Also to be analysed it the post-fit residuals to examine the effects of mismodeling. The temporal and spatial behaviour of these estimated terms will be examined for the different products applied to understand the unmodeled effects that introduced incorrect solution fixes. The number of reference stations examined would also be increased to further test the reliability of the transformed products under varying user conditions

## ACKNOWLEDGMENTS

Paul Collins, Jianghui Geng, and Denis Laurichesse are acknowledged for their valuable discussions and suggestions. The research was funded from the Natural Sciences and Engineering Research Council of Canada. The results presented are derived from data and products provided by Natural Resources Canada, Scripps Institution of Oceanography, Centre national d'études spatiales and the International GNSS Service.

## REFERENCES

- Aggrey JE (2015) Multi-gnss precise point positioning software architecture and analysis of glonass pseudorange biases. York University, Toronto, Ontario
- Bertiger W, Desai SD, Haines B, et al (2010) Single receiver phase ambiguity resolution with GPS data. *J Geod* 84:327–337. doi: 10.1007/s00190-010-0371-9
- CNES (2015) Le site du Centre national d'études spatiales. <https://cnes.fr/>.
- Collins P (2008) Isolating and estimating undifferenced GPS integer ambiguities. In: Proc. ION NTM. pp 720–732
- Collins P, Bisnath S (2011) Issues in ambiguity resolution for Precise Point Positioning. In: Proceedings of the 24th International Technical Meeting of the Satellite Division of The Institute of Navigation (ION GNSS 2011). pp 679–687
- Collins P, Bisnath S, Lahaye F, Héroux P (2010) Undifferenced GPS ambiguity resolution using the decoupled clock model and ambiguity datum fixing. *Navigation* 57:123–135.
- Ge M, Gendt G, Rothacher M, et al (2008) Resolution of GPS carrier-phase ambiguities in Precise Point Positioning (PPP) with daily observations. *J Geod* 82:389–399. doi: 10.1007/s00190-007-0187-4
- Geng J (2010) Rapid integer ambiguity resolution in GPS precise point positioning. University of Nottingham
- Geng J, Bock Y (2013) Triple-frequency GPS precise point positioning with rapid ambiguity resolution. *J Geod* 87:449–460. doi: 10.1007/s00190-013-0619-2
- Geng J, Meng X, Dodson AH, Teferle FN (2010) Integer ambiguity resolution in precise point positioning: method comparison. *J Geod* 84:569–581. doi: 10.1007/s00190-010-0399-x
- Geng J, Shi C, Ge M, et al (2012) Improving the estimation of fractional-cycle biases for ambiguity resolution in precise point positioning. *J Geod* 86:579–589.
- Geng J, Teferle FN, Shi C, et al (2009) Ambiguity resolution in precise point positioning with hourly data. *GPS Solut* 13:263–270. doi: 10.1007/s10291-009-0119-2
- Lannes A, Prieur J-L (2013) Calibration of the clock-phase biases of GNSS networks: the closure-ambiguity approach. *J Geod* 87:709–731. doi: 10.1007/s00190-013-0641-4
- Laurichesse D (2014) Phase biases for ambiguity resolution: from an undifferenced to an uncombined formulation.
- Laurichesse D, Mercier F (2007) Integer ambiguity resolution on undifferenced GPS phase measurements and its application to PPP. pp 839–848
- Laurichesse D, Mercier F, Berthias J-P, et al (2009) Integer ambiguity resolution on undifferenced GPS phase measurements and its application to PPP and satellite precise orbit determination. *Navigation* 56:135–149.
- Mercier F, Laurichesse D (2007) Receiver/Payload hardware biases stability requirements for undifferenced Widearea ambiguity blocking. In: Scientifics and fundamental aspects of the Galileo program Colloquium, Fall.
- Mervart L, Lukes Z, Rocken C, Iwabuchi T (2008) Precise Point Positioning with ambiguity resolution in real-time. In: Proceedings of ION GNSS. pp 397–405

- Montenbruck O, Schmid R, Mercier F, et al (2015) GNSS satellite geometry and attitude models. *Adv Space Res* 56:1015–1029. doi: 10.1016/j.asr.2015.06.019
- NRCan (2015) Natural Resources Canada. <https://www.nrcan.gc.ca>. Accessed 19 Jun 2015
- Scherneck H (2013) Ocean Tide Loading Provider. <http://froste.oso.chalmers.se/loading//index.html>. Accessed 2 Jan 2013
- Scripps (2015) Scripps Institution of Oceanography. <https://scripps.ucsd.edu/>. Accessed 19 Jun 2015
- Seepersad G (2012) Reduction of initial convergence period in GPS PPP data processing. York University, Toronto, Ontario
- Shi J, Gao Y (2013) A comparison of three PPP integer ambiguity resolution methods. *GPS Solut* 18:519–528. doi: 10.1007/s10291-013-0348-2
- Teunissen PJG, Khodabandeh A (2015) Review and principles of PPP-RTK methods. *J Geod* 89:217–240. doi: 10.1007/s00190-014-0771-3
- Teunissen PJ, Odijk D, Zhang B (2010) PPP-RTK: Results of CORS network-based PPP with integer ambiguity resolution. *J Aeronaut Astronaut Aviat Ser A* 42:223–230.
- Zhang B, Teunissen PJG, Odijk D (2011) A Novel Un-differenced PPP-RTK Concept. *J Navig* 64:S180–S191. doi: 10.1017/S0373463311000361